DOI: 10.1021/ic900585p

Inorganic Chemistry
Article

Injection, Transport, Absorption and Phosphorescence Properties of a Series of Blue-Emitting Ir(III) Emitters in OLEDs: a DFT and Time-Dependent DFT Study

Xiao-Na Li,[†,‡] Zhi-Jian Wu,[†] Zhen-Jun Si,[†] Hong-Jie Zhang,*[,†] Liang Zhou,[†,‡] and Xiao-Juan Liu[†]

[†]*State Key Laboratory of Rare Earth Resource Utilization, Changchun Institute of Applied Chemistry, Chinese Academy of Sciences, Changchun 130022, People's Republic of China, and* [‡]*Graduate School of the Chinese Academy of Sciences, Beijing, People's Republic of China*

Received March 25, 2009

Quantum-chemistry methods were explored to investigate the electronic structures, injection and transport properties, absorption and phosphorescence mechanism of a series of blue-emitting Ir(III) complexes {[$(F_2$-ppy$)_2$Ir(pta −X/pyN4)], where F_2-ppy = (2,4-difluoro)phenylpyridine; pta = pyridine-1,2,4-triazole; X = phenyl(**1**); *p*-tolyl (**2**); 2,6-difluororophenyl (**3**); $-CF_3$ (**4**), and pyN4 = pyridine-1,2,4-tetrazolate (**5**)}, which are used as emitters in organic light-emitting diodes (OLEDs). The mobility of hole and electron were studied computationally based on the Marcus theory. Calculations of Ionization potentials (IPs) and electron affinities (EAs) were used to evaluate the injection abilities of holes and electrons into these complexes. The reasons for the lower EL efficiency and phosphorescence quantum yields in **3**−**5** than in **1**and **2** have been investigated. These new structure−property relationships can guide an improved design and optimization of OLED devices based on blue-emitting phosphorescent Ir(III) complexes.

Introduction

Recently, phosphorescent transition-metal complexes with d^6 electron configuration such as Re(I),[1] Ru(II),[2] Os(II),[3] and Ir(III)[4] have attracted considerable attention because of their intriguing photophysical, photochemical, and potential practical applications as organic light emitting devices (OLEDs) and biological labeling reagents.[5] More specifically, these transition metal complexes would display bright phosphorescent emission spanning the whole visible spectra, making them suitable to serve as ideal phosphors for OLED applications. Among them, iridium(III) complexes are regarded as the most effective materials in OLEDs because of their high thermal stability, short lifetime in excited states, and strong spin−orbit coupling effect of heavy metal, which can, to a large extent, partially remove the spin-forbidden nature of the $T_1 \rightarrow S_0$ radiative relaxation.

Among these Ir(III) complexes, green- and red-emitting species have been known for years and successfully fabricated as emitters in OLEDs with high quantum efficiency.[6] However, achieving room-temperature blue phosphorescence with high quantum efficiency remains as a challenge.[7] One major challenge lies in the selection of suitable chelate ligands with sufficiently large ligand-centered (LC) $\pi \rightarrow \pi^*$ transition energies and/or metal-to-ligand charge transfer (MLCT) energies. Previously, the emission wavelength can be easily tuned mostly through the structure variation of phenylpyridine (C^N) ligand, while changing the ancillary ligand leads only to a minor shift.[8] Recently, 2-(2,4-difluorophenyl)pyridine

*To whom correspondence should be addressed. E-mail: hongjie@ciac.jl.cn. Phone: +86 431 85262127. Fax: +86 431 85698041.

(1) (a) Dunn, A. R.; Bittner, W. B.; Winkler, J. R.; Getzoff, E. D.; Stuehr, D. J.; Gray, H. B. *J. Am. Chem. Soc.* **2005**, *127*, 5169–5173. (b) Lo, K. K.-W.; Lau, J. S.-Y.; Fong, V. W.-Y. *Organometallics* **2004**, *23*, 1098–1106.

(2) (a) Fodor, L.; Lendvay, G.; Horváth, A. *J. Phys. Chem. A* **2007**, *111*, 12891–12900. (b) Alary, F.; Pasqua, M. B.; Heully, J.-L.; Marsden, C. J.; Vlcendo, P. *Inorg. Chem.* **2008**, *47*, 5259–5266.

(3) (a) Chou, P. T.; Chi, Y. *Chem.—Eur. J.* **2007**, *13*, 380–395. (b) Chou, P. T.; Chi, Y. *Eur. J. Inorg. Chem.* **2006**, 3319–3332.

(4) (a) Lin, J. J.; Liao, W. S.; Huang, H. J.; Wu, F. I.; Cheng, C. H. *Adv. Funct. Mater.* **2008**, *18*, 485–491. (b) Zhou, G. J.; Ho, C. L.; Wong, W. Y.; Wang, Q.; Ma, D. G.; Wang, L. X.; Lin, Z. Y.; Marder, T. B.; Beeby, A. *Adv. Funct. Mater.* **2008**, *18*, 499–511.

(5) Yin, B. L.; Niemeyer, F.; Williams, J. A. G.; Jiang, J.; Boucekkine, A.; Toupet, L.; Bozec, H. L.; Guerchais, V. *Inorg. Chem.* **2006**, *45*, 8584–8596.

(6) (a) Adachi, C.; Baldo, M. A.; Forrest, S. R.; Thompson, M. E. *Appl. Phys. Lett.* **2000**, *77*, 904–906. (b) Hua, F.; Kinayyigit, S.; Cable, J. R.; Castellano, F. N. *Inorg. Chem.* **2005**, *44*, 471–473. (c) Kavitha, J.; Chang, S. Y.; Chi, Y.; Yu, J. K.; Hu, Y. H.; Chou, P. T.; Peng, S. M.; Lee, G. H.; Tao, Y. T.; Chien, C. H.; Carty, A. J. *Adv. Funct. Mater.* **2005**, *15*, 223–229. (d) Anthopoulos, T. D.; Frampton, M. J.; Namdas, E. B.; Burn, P. L.; Samuel, I. D. W. *Adv. Mater.* **2004**, *16*, 557–560.

(7) (a) Stufkens, D. J.; Vlcek, A., Jr. *Coord. Chem. Rev.* **1998**, *177*, 127–179. (b) Ranjan, S.; Lin, S. Y.; Hwang, K. C.; Chi, Y.; Ching, W. L.; Liu, C. S. *Inorg. Chem.* **2003**, *42*, 1248–1255.

(8) (a) Lamansky, S.; Djurovich, P.; Murphy, D.; Razzaq, F. A.; Kwong, R.; Tsyba, I.; Bortz, M.; Mui, B.; Bau, R.; Thompson, M. E. *Inorg. Chem.* **2001**, *40*, 1704–1711. (b) Lamansky, S.; Djurovich, P.; Murphy, D.; Razzaq, F. A.; Lee, H. E.; Adachi, C.; Burrows, P. E.; Forrest, S. R.; Thompson, M. E. *J. Am. Chem. Soc.* **2001**, *123*, 4304–4312. (c) Grushin, V. V.; Herron, N.; LeCloux, D. D.; Marshall, W. J.; Petrov, V. A.; Wang, Y. *Chem. Commun.* **2001**, 1494–1495. (d) Tsuzuki, T.; Shirasawa, N.; Suzuki, T.; Tokito, S. Z. *Adv. Mater.* **2003**, *15*, 1455–1458. (e) Hwang, F. M.; Chen, H. Y.; Chen, P. S.; Liu, C. S.; Chi, Y.; Shu, C. F.; Wu, F. I.; Chou, P. T.; Peng, S. M.; Lee, G. H. *Inorg. Chem.* **2005**, *44*, 1344–1353.

Published on Web 07/10/2009

(F_2-ppy) has been the main potent ligand in providing short emission wavelength, and therefore, the ancillary ligand becomes the decisive structural factor for blue color of iridium complexes.[9] In this aspect, strong field ligands are usually selected as ancillary ligands such as cyanide, carbonyl, phosphine, and NHC carbene ligand with an aim to increase the HOMO−LUMO energy gaps.[10] These strong field ligands can destabilize the metal-centered (MC) dd states, and consequently reduce the radiationless deactivation. For example, a series of new blue-emitting complexes $[Ir(C^\wedge N)(PR_3)_2LL']^{0,+}$($C^\wedge N$ = ppy, F_2ppy, F_2Meppy; $PR_3 = PPh_3$, PPh_3Me) emit deep- and sky-blue light when L and L′ are strong field ligands such as H^-, CO, and CN^- and medium-field ligand MeCN.[11] Ancillary ligands such as picolinic acid (pic) and 2-pyridylazoles can alter the excited-state properties through altering the MLCT energy mainly by changing the highest occupied molecular orbital (HOMO) energy level because the HOMO is mainly localized on the picolinic or 2-pyridylazoles ligands. For 2-pyridylazoles ligands as an example, the strong σ-donor property of azolate, together with the π-accepting ability of the second pyridyl fragment,[12] may provide a synergism of the electron delocalization so that the electron density is transferred from azolate to the metal ion and back to the pyridyl side of the ligand, thus enhance the chelate interaction. This strong metal−ligand interaction results in the orbital composition of the HOMO mainly localized on the pic ligand,[13] and the lowest unoccupied molecular orbital (LUMO) is localized on the main ligand such as ppy, F_2-ppy, which is contrast to the conventional $[Ir(C^\wedge N)_2(N^\wedge N)]^+$ complexes, in which the HOMO consists principally of a mixture of phenyl π-and Ir d-orbital and the LUMO is localized largely on bpy π*-orbitals.[14] Therefore, by changing the substitutive group or substituent position on these ancillary ligands can make more change in HOMO than LUMO and furthermore change the excited state energy.

In contrast to the wide experimental investigations, quantum-chemistry study on blue-emitting Ir complexes is limited.[15] To foresee new structure−property relationships and help to improve the design of OLEDs based on blue-emitting iridium(III) complexes, we theoretically investigated the injection, transport, absorption, and phosphorescence properties for a series of blue-emitting iridium(III) complexes $Ir(F_2\text{-ppy})_2$(pta-X/pyN4), where F_2-ppy = (2,4-difluoro)-phenylpyridine; pta = pyridine-1,2,4-triazole; X = phenyl(**1**); *p*-tolyl (**2**); 2,6-difluororophenyl (**3**); $-CF_3$ (**4**) and pyN4 = pyridine-1,2,4-tetrazolate (**5**)[16,17] using density functional theory (DFT) and time-dependent density functional theory (TD-DFT). We hope that the study could provide useful information for the design of new phosphors in OLEDs with high electroluminescence (EL) efficiency and high phosphorescence quantum yields.

Computational Details

The ground-state and the lowest-lying triplet excited-state geometries were optimized by the DFT[18] method with Becke's LYP (B3LYP) exchange-correlation functional[19] and the configuration interaction with single excitations (CIS)[20] approach, respectively. There were no symmetry constraints on these complexes. At the respective optimized geometries of ground and excited states, TDDFT[21] calculations using the B3LYP functional with the same basis set, associated with the polarized continuum model (PCM)[22] in dichloromethane (CH_2Cl_2) media, were carried out to obtain the vertical excitation energies of singlet (S_n) and triplet (T_n) states. Recent calculations with TDDFT method for transition-metal complexes have supported its credibility and gave good agreement with experimental spectra.[23]

In the calculation, the quasi-relativistic pseudopotentials of Ir atoms proposed by Hay and Wadt[24] with 17 valence electrons were employed, and a "double-ξ"quality basis set LANL2DZ was adopted as the basis set. 6-31G(d) basis set was used on C, H, N, O, and F atoms in all the calculations, with the exception for electronic affinities (EA), in which, to describe EA more properly, we further optimized the neutral and the anionic species with 6-31+G(d) basis sets. Furthermore, the stable configurations of these complexes can be confirmed by frequency analysis, in which no imaginary frequency was found for all configurations at the energy minima. As a check for the presence of spin contamination, we compare the calculated value of total spin $\langle S^2\rangle$ with the experimental value. If there is no spin contamination, $\langle S^2\rangle$ should equal $s(s+1)$, where s equals 1/2 times the number of unpaired electrons. From the experience with organic

(9) (a) Li, J.; Djurovich, P. I.; Alleyne, B. D.; Tsyba, I.; Ho, N. N.; Bau, R.; Thompson, M. E. *Polyhedron* **2004**, *23*, 419–428. (b) Yang, C. H.; Cheng, Y. M.; Chi, Y.; Hsu, C. J.; Fang, F. C.; Wong, K. T.; Chou, P. T.; Chang, C. H.; Tsai, M. H.; Wu, C. C. *Angew. Chem., Int. Ed.* **2007**, *46*, 2418–2421. (c) Chiu, Y. C.; Chi, Y.; Hung, J. Y.; Cheng, Y. M.; Yu, Y. C.; Chung, M. W.; Lee, G. H.; Chou, P. T.; Chen, C. C.; Wu, C. C.; Hsieh, H. Y. *ACS Appl. Mater. Int.* **2009**, *1*, 433–442.

(10) (a) Nazeeruddin, M. K.; Baker, R. H.; Berner, D.; Rivier, S.; Zuppiroli, L.; Graetzel, M. *J. Am. Chem. Soc.* **2003**, *125*, 8790–8797. (b) Lee, C. L.; Das, R. R.; Kim, J. J. *Chem. Mater.* **2004**, *16*, 4642–4646. (c) Chang, C. F.; Cheng, Y. M.; Chi, Y.; Chiu, Y. C.; Lin, C. C.; Lee, G. H.; Chou, P. T.; Chen, C. C.; Chang, C. H.; Wu, C. C. *Angew. Chem., Int. Ed.* **2008**, *47*, 4542–4545.

(11) Eum, M. S.; Chin, C. S.; Kim, S. Y.; Kim, C.; Kang, S. K.; Hur, N. H.; Seo, J. H.; Kim, G. Y.; Kim, Y. K. *Inorg. Chem.* **2008**, *47*, 6289–6295.

(12) Hage, R.; Haasnoot, J. G.; Reedijk, J.; Wang, R.; Vos, J. G. *Inorg. Chem.* **1991**, *30*, 3263–3269.

(13) Gu, X.; Fei, T.; Zhang, H. Y.; Xu, H.; Yang, B.; Ma, Y. G.; Liu, X. D. *J. Phys. Chem. A* **2008**, *112*, 8387–8393.

(14) (a) Hay, P. J. *J. Phys. Chem. A* **2002**, *106*, 1634–1641. (b) Zhao, Q.; Liu, S. J.; Shi, M.; Wang, C. M.; Yu, M. X.; Li, L.; Li, F. Y.; Yi, T.; Huang, C. H. *Inorg. Chem.* **2006**, *45*, 6152–6160.

(15) (a) Terki, R.; Simoneau, L. P.; Rochefort, A. *J. Phys. Chem. A* **2009**, *113*, 534–541. (b) Liu, T.; Xia, B. H.; Zhou, X.; Zheng, Q. C.; Pan, Q. J.; Zhang, H. X. *Theor. Chem. Acc.* **2008**, *121*, 155–164.

(16) Orselli, E.; Kottas, G. S.; Konradsson, A. E.; Coppo, P.; Fröhlich, R.; De Cola, L.; Dijken, A. V.; Büchel, M.; Börner, H. *Inorg. Chem.* **2007**, *46*, 11082–11093.

(17) Yeh, S. J.; Wu, M. F.; Chen, C. T.; Song, Y. H.; Chi, Y.; Ho, M. H.; Hsu, S. F.; Chen, C. H. *Adv. Mater.* **2005**, *17*, 285–289.

(18) Runge, E.; Gross, E. K. U. *Phys. Rev. Lett.* **1984**, *52*, 997–1000.

(19) Mayo, S. L.; Olafson, B. D.; Goddard, W. A. III *J. Phys. Chem.* **1990**, *94*, 8897–8909.

(20) Foresman, J. B.; Gordon, M. H.; Pople, J. A.; Frisch, M. J. *J. Phys. Chem.* **1992**, *96*, 135–149.

(21) (a) Autschbach, J.; Ziegler, T.; Gisbergen, S. J. A.; Baerends, E. J. *J. Chem. Phys.* **2002**, *116*, 6930–6940. (b) Helgaker, T.; Jørgensen, P. *J. Chem. Phys.* **1991**, *95*, 2595–2601. (c) Bak, K. L.; Jørgensen, P.; Helgaker, T.; Rund, K.; Jensen, H. J. A. *J. Chem. Phys.* **1993**, *98*, 8873–8887.

(22) Mennucci, B.; Tomasi, J. *J. Chem. Phys.* **1997**, *106*, 5151–5158.

(23) (a) Kirgan, R. A.; Rillema, D. P. *J. Phys. Chem. A* **2007**, *111*, 13157–13162. (b) Villegas, J. M.; Stoyanov, S. R.; Huang, W.; Rillema, D. P. *Inorg. Chem.* **2005**, *44*, 2297–2309. (c) Fantacci, S.; Angelis, F. D.; Selloni, A. *J. Am. Chem. Soc.* **2003**, *125*, 4381–4387. (d) Censo, D. D.; Fantacci, S.; Angelis, F. D.; Klein, C.; Evans, N.; Kalyanasundaram, K.; Bolink, H. J.; Grätzel, M.; Nazeeruddin, M. K. *Inorg. Chem.* **2008**, *47*, 980–989. (e) Nazeeruddin, M. K.; Angelis, F. D.; Fantacci, S.; Selloni, A.; Viscardi, G.; Liska, P.; Ito, S.; Takeru, B.; Grätzel, M. *J. Am. Chem. Soc.* **2005**, *127*, 16835–16847. (f) Barolo, C.; Nazeeruddin, M. K.; Fantacci, S.; Censo, D. D.; Comte, P.; Liska, P.; Viscardi, G.; Quagliotto, P.; Angelis, F. D.; Grätzel, M. *Inorg. Chem.* **2006**, *45*, 4642–4653. (g) Shi, L. L.; Liao, Y.; Zhao, L.; Su, Z. M.; Kan, Y. H.; Yang, G. C.; Yang, S. Y. *J. Organomet. Chem.* **2007**, *692*, 5368–5374.

(24) (a) Hay, P. J.; Wadt, W. R. *J. Chem. Phys.* **1985**, *82*, 270–283. (b) Hay, P. J.; Wadt, W. R. *J. Chem. Phys.* **1985**, *82*, 299–310.

molecule calculations, the spin contamination can be negligible if the calculated value of $\langle S^2 \rangle$ differs from $s(s+1)$ by less than 10%. All the calculated $\langle S^2 \rangle$ values in this paper for open-shell systems change in the range 0.7569−0.7647, which differs 0.9%∼2.0% from the experimental value of 0.75. Therefore, the spin contamination can be said to be negligible in these calculations. All the calculations were performed with the Gaussian 03 software package[25] on the Origin/3900 server.

Results and Discussion

Geometries in the Ground State S_0 and Triplet Excited State T_1. The sketch map of the five complexes is presented in Figure 1, and the optimized ground-state geometrical structures for **1** and **3** are shown in Figure 2 along with the numbering of some key atoms. The main geometry structural parameters are summarized in Table 1 together with the X-ray crystal structure data of **2**.[16] All complexes show a pseudo-octahedral coordination around the metal centers with the two N atoms (N3 and N5) from F_2-ppy ligands residing at the *trans* location, and C4 and C6 at the *cis* location. The introduction of different substituents on the ending phenyl ring cause only minor differences of geometrical parameters for **1**−**3**. While the calculated bond lengths of Ir−N1 and Ir−N2 in **4** and generally all bond lengths in **5** are longer than in **1**−**3** and with the largest differences focused on Ir−N1 and Ir−N2. These elongated bond lengths result from the electron-withdrawing effect and the enhanced interannular π-conjugation of tetrazolate ring in **4** and **5**, respectively. For **5**, the enhanced π-conjugation consequently contracts the tetrazolate ring and weakens the interaction between tetrazolate moiety and the metal. The difference of bond angles among these complexes is negligible. Generally speaking, the calculated results of **1**−**5** are in agreement with the corresponding X-ray results. The slight elongation of the calculated metal−ligand distances compared with the experimental values can be attributed to the crystal packing in the crystalline state.

It is interesting to note that the Ir−N1 bond lengths are shorter than the Ir−N2 ones. For **1**−**3**, this can be rationalized by the presence of the ending phenyl ring on triazole moiety which can extend the π-electron delocalization among the triazole moiety and the phenyl ring, and therefore, improve the cooperative effect.[26] This is also reflected in the Ir−C4 and Ir−C6 bond lengths, in which the Ir−C6 bond length is longer than the Ir−C4 bond length. The longer Ir−C6 bond length is believed to be caused by the stronger Ir−N1 bonding interaction, which eventually weakened the Ir−C6 bond at the *trans* disposition. For **4** and **5**, the main reason is that the π-accepting ability of triazole and tetrazolate ring is greater than that of the pyridine ring, which can also increase the cooperative effect.[26]

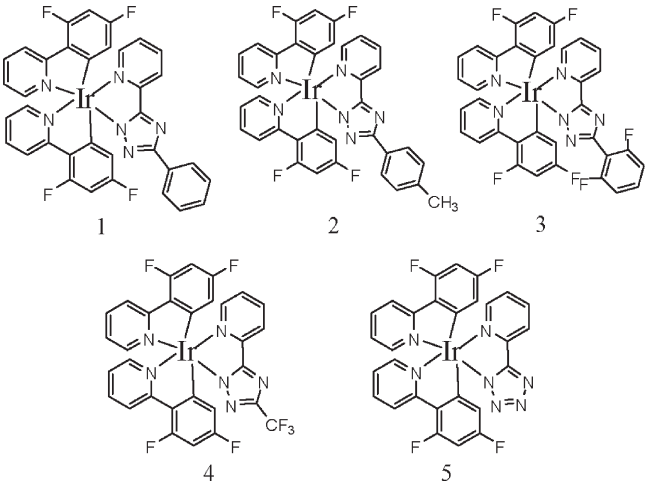

Figure 1. Sketch structures of the five complexes.

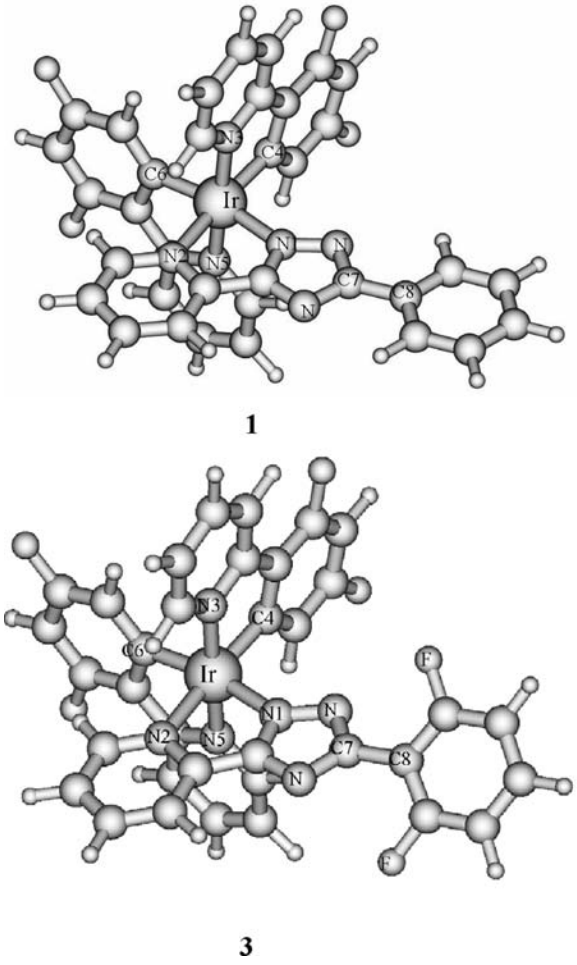

Figure 2. Optimized structures of **1** and **3** in the ground states at DFT/B3LYP/LANL2DZ level.

(25) Frisch, M. J.; Trucks, G. W.; Schlegel, H. B.; Scuseria, G. E.; Robb, M. A.; Cheeseman, J. R.; Montgomery, J. A., Jr.; Vreven, T.; Kudin, K. N.; Burant, J. C.; Millam, J. M.; Iyengar, S. S.; Tomasi, J.; Barone, V.; Mennucci, B.; Cossi, M.; Scalmani, G.; Rega, N.; Petersson, G. A.; Nakatsuji, H.; Hada, M.; Ehara, M.; Toyota, K.; Fukuda, R.; Hasegawa, J.; Ishida, M.; Nakajima, T.; Honda, Y.; Kitao, O.; Nakai, H.; Klene, M.; Li, X.; Knox, J. E.; Hratchian, H. P.; Cross, J. B.; Adamo, C.; Jaramillo, J.; Gomperts, R.; Stratmann, R. E.; Yazyev, O.; Austin, A. J.; Cammi, R.; Pomelli, C.; J. Ochterski, W.; Ayala, P. Y.; Morokuma, K.; Voth, G. A.; Salvador, P.; Dannenberg, J. J.; Zakrzewski, V. G.; Dapprich, S.; Daniels, A. D.; Strain, M. C.; Farkas, O.; D. Malick, K.; A. Rabuck, D.; Raghavachari, K.; Foresman, J. B.; Ortiz, J. V.; Cui, Q.; Baboul, A. G.; Clifford, S.; Cioslowski, J.; Stefanov, B. B.; Liu, G.; Liashenko, A.; Piskorz, P.; Komaromi, I.; Martin, R. L.; Fox, D. J.; Keith, T.; Al-Laham, M. A.; Peng, C. Y.; Nanayakkara, A.; Hallacombe, M.; Gill, CP. M. W.; Johnson, B.; Chen, W.; Wong, M. W.; Gonzalez, C.; and Pople, J. A. *Gaussian 03*, revision C.02; Gaussian, Inc.: Wallingford, CT, 2004.

(26) Zhou, X.; Ren, A. M.; Feng, J. K. *J. Organomet. Chem.* **2005**, *690*, 338–347.

Table 1. Main Optimized Geometry Structural Parameters of **1**−**5** in the Ground and the Lowest Lying Triplet States at the B3LYP and CIS Level, Respectively, Together with the Experimental Values of **2**

	1		**2**		**3**		**4**		**5**		exptl[16]
	S_0	T_1	S_0	T_1	S_0	T_1	S_0	T_1	S_0	T_1	**2**
						Bond Length (Å)					
Ir−N1	2.151	2.141	2.150	2.140	2.150	2.151	2.155	2.158	2.159	2.161	2.100
Ir−N2	2.252	2.245	2.251	2.244	2.252	2.274	2.256	2.277	2.259	2.285	2.177
Ir−N3	2.073	2.103	2.073	2.103	2.074	2.103	2.074	2.103	2.076	2.103	2.041
Ir−C4	2.013	2.031	2.013	2.031	2.012	2.026	2.012	2.026	2.013	2.025	2.007
Ir−N5	2.072	2.099	2.072	2.099	2.072	2.088	2.073	2.089	2.073	2.089	2.043
Ir−C6	2.026	2.050	2.026	2.050	2.026	2.050	2.025	2.047	2.023	2.046	2.019
C7−C8	1.469	1.472	1.468	1.469	1.472	1.480	1.451	1.494			1.462
						Bond Angle (deg)					
N3−Ir−N5	174.7	174.7	174.7	174.7	174.8	175.0	174.7	174.9	174.8	174.9	173.7
N3−Ir−C6	96.9	97.3	97.0	97.3	97.1	97.2	96.9	97.1	97.0	97.1	97.5
						Dihedral Angle (deg)					
N1−N2−Ir−N3	−87.2	−86.4	−87.4	−86.4	−86.7	−86.7	−86.7	−86.6	−87.1	−86.7	−86.3
C4−N3−Ir−C6	−89.9	−88.9	−90.0	−88.9	−89.9	−89.1	−90.0	−89.1	−89.6	−89.1	−84.9

The calculated geometrical parameters of the lowest-lying triplet excited states of **1**−**5** are also listed in Table 1. Table 1 shows that the variation of bond distances for **1** and **2** are different from that of **3**−**5**. The Ir−N1 and Ir−N2 bonds for **1** and **2** are contracted in T_1 states compared with those in S_0 states, while **3**−**5** have the opposite trend. For all the five complexes, other bond lengths are elongated in T_1 states, and the variation degree of **1** and **2** is larger than of **3**−**5**. These changes indicate that the interaction between metal and pta will be strengthened in T_1 states for **1** and **2** compared with the interaction between metal and F_2-ppy, and this interaction has the opposite trend for **3**−**5**. Because of the stronger interaction between F_2-ppy and the metal in **3**−**5**, F_2-ppy ligand will have greater effect on frontier molecular orbitals (FMOs) in both the ground state and the excited state. Furthermore, this different strength between the metal and the F_2-ppy or pta/pyN4 ligand will result in different electron transition characters.

Molecular Orbital Properties. It is known that the observed differences in optical and chemical properties of these complexes depend mainly on the changes of the ground-state electronic structure. The concept of emission color turning by grafting various substituents relies on the fact that the lowest excited state is relatively well described as a HOMO to LUMO transition in a given ligand.[27] Therefore, we will discuss in detail the ground-state electronic structure with the special emphasis on the HOMO and LUMO distribution, energy levels, and energy gaps. The FMO compositions of **1**−**5** are given in Tables S1−S5, Supporting Information. The ancillary ligands are denoted as pta/pyN4, and substituents are donated as ph, Me-ph, F_2-ph, CF_3 for **1**−**4**, respectively. The HOMO and LUMO distribution, energy levels, and energy gaps are plotted in Figure 3.

For **1**, Figure 3 and Table S1, Supporting Information show that the HOMO mainly resides on the pta moiety, and the composition extends to the ending phenyl moiety with the proportion of 29.9%. The composition on dπ is only 11.3% (9.5% d_{xz}) and the metal d orbital is an antibonding combination with the pta π-orbital. The HOMO of **2** has the similar distribution to **1.** The attached electron-donating group $-CH_3$ pulls the electron density moving toward the ending substituent with the proportion on the ancillary ligand increased up to 37.7%. For **3**, the HOMO extends over the d_{z^2} orbital of the Ir atom, the phenyl moiety of two F_2-ppy ligands, the pta ligand, and the ending phenyl ring, which is more evenly distributed. The main reason resulting in this different distribution from **1** and **2** is due to the torsion angle of 39.6° between the triazole moiety and the ending phenyl ring, which breaks the π-conjugation across the triazole and the ending phenyl ring to a large extent. Therefore, this weakens the interaction between them and causes the slight shift of the electron density from the pta moiety to the metal and eventually to the F_2-ppy moiety. Our explanation has been demonstrated by the recent report on a series of similar complexes, among which one complex (similar to **3** but with two F atom attached at 3 and 5 positions) does not cause obvious orbital composition localized on the F_2-ppy moiety because of the absence of this torsion.[28] The HOMOs of **4** and **5** are mainly a metal d and a F_2-ppy based π-orbital, and the composition coming from pta/pyN4 moiety has vanished. This is consistent with the generally longer metal-pta/pyN4 bond lengths in **4** and **5**, which weakens the interaction between metal and pta/pyN4 moiety, and consequently cause the negligible distribution localized on pta/pyN4 moiety. The LUMO for **1**—**3** is predominantly of F_2-ppy π*-orbital character, while the LUMO for **4** and **5** is more evenly distributed covering the F_2-ppy and pta/pyN4 moieties. Details of other orbital compositions can be seen from Tables S1−S5, Supporting Information.

Moreover, the energy levels of HOMO and LUMO are greatly influenced by different substituents on the ancillary ligands. Figure 3 shows that the complexes with phenyl ring substituents (**1**−**3**) have generally the higher HOMO and LUMO levels. Among **1**−**3**, electron-donating

(27) Avilov, I.; Minoofar, P.; Cornil, J.; De Cola, L. *J. Am. Chem. Soc.* **2007**, *129*, 8247–8258.

(28) Orselli, E.; Albuquerque, R. Q.; Fransen, P. M.; Fröhlich, R.; Janssen, H. M.; De Cola, L. *J. Mater. Chem.* **2008**, *18*, 4579–4590.

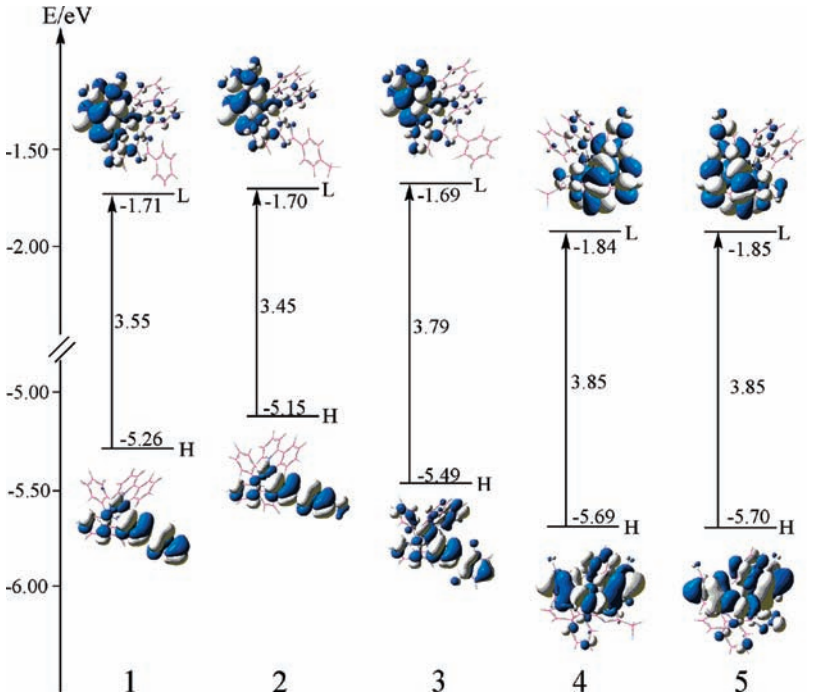

Figure 3. Presentation of the energy levels, energy gaps and orbital composition distribution of the HOMO and the LUMO for the five complexes.

group $-CH_3$ (**2**) can destabilize both of the HOMO and LUMO energy levels. While electron-withdrawing group, $-F$ (**3**) greatly stabilizes the HOMO energy and destabilizes the LUMO level, which results in the largest H−L gap of 3.79 eV among the three complexes. While in **4** and **5**, the $-CF_3$ substituent and tetrazolate ring can stabilize both HOMO and LUMO energies to a large extent compared with **1**−**3**, and both of them have similar levels. The raised HOMO energy levels of **1**−**3** will benefit the hole injection, while the slightly increased LUMO levels will decrease the electron injection ability, and **4** and **5** have the opposite trend. These relative HOMO and LUMO energy levels will guide to compare the EL efficiency of OLEDs among these complexes, and this will be discussed in the next section.

Ionization Potentials (IP) and Electronic Affinities (EA). The device performance of OLEDs depends on the charge injection, transfer, and balance, as well as the exciton confinement in a device. In this section, we present ionization potentials (IP), electron affinities (EA), and reorganization energy (λ) calculated for the five complexes, together with hole extraction potential (HEP), electron extraction potential (EEP), and "small-polaron" stabilization energy (SPE). The IP and EA can be either for vertical excitations (v; at the geometry of neutral molecule) or adiabatic excitations (a; optimized structure for both the neutral and charged molecule). The IP and EA are used to evaluate the energy barrier for the injection of holes and electrons, and the reorganization energy is used to evaluate the charge transfer rate and balance. For photoluminescent materials, the lower IP of the emitter, the easier the entrance of holes from the hole-transport layer (HTL) to the emitter; and the higher the EA of the emitter, the easier the entrance of electrons from the electron-transport layer (ETL). For IP and EA calculations, we did not include the solvent polarization of the surrounding medium. In the case of solid-state photoelectronic devices such as LEDs, however, this solvent factor can be negligible, and this comparison trend of charge injection abilities in IP and EA has been demonstrated credible by many reports,[29] and it is the same case for SPE. In addition, HEP is the energy difference from M (neutral molecule) to M^+ (cationic), using M^+ geometric structure in the calculation, and EEP is energy difference from M to M^- (anionic), using M^- geometric structure in the calculation. Furthermore, SPE is used to estimate self-trapping energies of charge in the materials, which is the energy gain of the excess electron because of structural relaxation, that is, the difference between EA(a) and EA(v) (for electron).

Table 2. Ionization Potentials, Electron Affinities, Extraction Potentials, Internal Reorganization Energies, and "Small-Polaron" Stabilization Energy for the Five Complexes (in eV) Calculated at DFT/B3LYP/LANL2DZ Level

	IP(v)	IP(a)	HEP	SPE(h)	EA(v)	EA(a)	EEP	SPE(e)	λ_{hole}	$\lambda_{electron}$
1	6.45	6.35	6.35	0.10	0.98	1.05	1.05	0.07	0.10	0.07
2	6.38	6.24	6.25	0.14	0.96	1.03	1.03	0.07	0.14	0.07
3	6.62	6.46	6.46	0.16	0.94	1.02	1.02	0.08	0.16	0.07
4	6.94	6.80	6.82	0.14	1.11	1.19	1.19	0.08	0.12	0.08
5	6.95	6.80	6.82	0.15	1.08	1.15	1.15	0.07	0.13	0.07

In Table 2, the calculated IP (both vertical and adiabatic) values increase in the following order: **2** < **1** < **3** < **4** < **5**. This indicates that the difficulties of hole injection from HTL to these complexes gradually increase, and this order is consistent with the trend of HOMO energy levels. By analysis of EA values, complexes **4** and **5** more easily accept an

(29) (a) Shi, L. L.; Liao, Y.; Yang, G. C.; Su, Z. M.; Zhao, S. S. *Inorg. Chem.* **2008**, *47*, 2347–2355. (b) Liao, Y.; Yang, G. C.; Feng, J. K.; Shi, L. L.; Yang, S. Y.; Yang, L.; Ren, A. M. *J. Phys. Chem. A* **2006**, *110*, 13036–13044. (c) Yu, G.; Yin, S. W.; Liu, Y. Q.; Shuai, Z. G.; Zhu, D. B. *J. Am. Chem. Soc.* **2003**, *125*, 14816–14824. (d) Yang, G. C.; Su, T.; Shi, S. Q.; Su, Z. M.; Zhang, H. J.; Wang, Y. *J. Phys. Chem. A* **2007**, *111*, 2739–2744. (e) Liu, Y. L.; Feng, J. K.; Ren, A. M. *J. Phys. Chem. A* **2008**, *112*, 3157–3164.

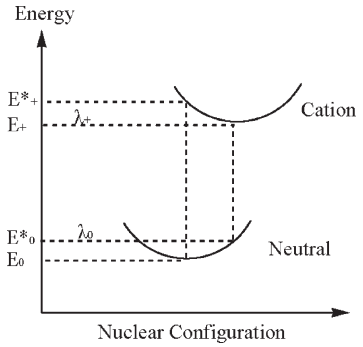

Figure 4. Schematic description of internal reorganization energy for hole transfer.

electron than **1**−**3**, and this trend is also consistent with the order of the LUMO energy levels.

According to the Marcus/Hush model,[30] the charge (hole or electron) transfer rate k can be expressed by the following formula:

$$k = \left(\frac{\pi}{\lambda k_B T}\right)^{1/2} \frac{V^2}{\hbar} \exp\left(-\frac{\lambda}{4k_B T}\right) = A \exp\left(-\frac{\lambda}{4k_B T}\right) \quad (1)$$

where T is the temperature, k_B is the Boltzmann constant, λ is the reorganization energy, and V is the coupling matrix element between the ions and molecules which is dictated by the overlap of orbitals. It can be seen from eq 1 that there are two factors λ and V that determine the transfer rate k. However, the intermolecular charge transfer range in the solid state is rather narrow and V is very limited; therefore, the mobility of charges has been demonstrated to be dominantly related to the internal reorganization energy λ for OLEDs materials.[31] The reorganization energy λ (herein the internal reorganization energy obtained by ignoring any environmental relaxation and changes) for hole transfers can be expressed as follows:[32]

$$\lambda_{hole} = \lambda_0 + \lambda_+ = (E^*_0 - E_0) + (E^*_+ - E_+) = IP(v) - HEP \quad (2)$$

as illustrated in Figure 4, E_0 and E_+ represent the energies of the neutral and cationic species in their lowest energy geometries, respectively, while E^*_0 and E^*_+ represent the energies of the neutral and cationic species with the geometries of the cationic and neutral species, respectively, which is equal to the difference between vertical IP and hole extraction energy HEP. In this way, λ for electron transfer can be expressed similar to that for hole transfer. As emitting layer materials, it needs to achieve hole and electron injection balance. Table 2 shows that the reorganization energies for hole transport (λ_{hole}) are slightly larger than those for electron transport ($\lambda_{electron}$), which reveals that the electron-transporting performance of these complexes is slightly better than that for hole transport. However, the differences between λ_{hole} and $\lambda_{electron}$ for these complexes are smaller than or comparable with many photoluminescent transition-metal complexes and organic molecules;[33] therefore, they are suitable as emitters in OLEDs. Highly important, it is essential to compare the EL efficiency of OLEDs among these five complexes, and therefore to facilitate the readers to catch up with the core subjects regarding the choice of ancillary ligands and different substituents suited for enhancing the performance of OLEDs. Table 2 shows that the hole injection barriers from HTL to emitters are smallest for **2**, slightly larger for **1** and **3**, and largest for **4** and **5**, while the electron injection abilities of **1**−**3** and **4**−**5** are almost equivalent, respectively, because of their very similar LUMO levels. In addition, the higher HOMO level can provide a more stable potential well for hole trapping. Therefore, we suppose that **1** and **2** have higher EL efficiency resulting from the improved ease of hole injection and electron trapping abilities, which can induce a build-in field in the EL layer and further accelerate the electron injection from ETL[34] than **3**−**5**. This can be seen from the little smaller electron trapping energies (SPE) of 0.07 eV for **1** and **2** than 0.08 eV for **3** and **4**, and comparable to **5** in Table 2.[35,36]

Absorption in CH_2Cl_2 Media. The calculated absorption spectra associated with their oscillator strengths, assignment, configurations, excitation energies, and CI coefficients are listed in Table 3. For clarity, only the most leading excited states (with larger CI coefficients) are listed. The fitted Gaussian type absorption curve is depicted in Figure 5.

In experiment, absorption spectra show intense features below 340 nm and less intense features in the range of 340−450 nm. Obviously, the calculated absorption spectra can reproduce well the experimental features in terms of band positions, intensities, and separations. The lowest transition energies follow the order: **5**∼**4** > **3** > **1** > **2**. An obvious blue shift of **4** and **5** compared with **1**−**3** is observed, and **3** is again blue-shifted compared with **1** and **2**. This is consistent with the variation rule of the energy gaps because the HOMO→LUMO transition configurations are predominantly $S_0 \rightarrow S_1$ transitions. From the above discussion on FMOs, the lowest lying absorptions are characterized as MLCT[d(Ir)→π^*(F_2-ppy/pta/pyN4)]/LLCT [π(pta/ph/F_2-ppy)→π^*(F_2-ppy/pta/pyN4)], and/or ILCT[π(F_2-ppy)→π^*(F_2-ppy)], with the exception of **2**, which is mainly the transition localized

(30) (a) Hush, N. S. *J. Chem. Phys.* **1958**, *28*, 962–972. (b) Marcus, R. A. *Rev. Mod. Phys.* **1993**, *62*, 599–610. (c) Marcus, R. A. *J. Chem. Phys.* **1956**, *24*, 966–978.

(31) (a) Malagoli, M.; Brédas, J. L. *Chem. Phys. Lett.* **2000**, *327*, 13–17. (b) Lin, B. C.; Cheng, C. P.; Ping, Z.; Lao, M. *J. Phys. Chem. A* **2003**, *107*, 5241–5251. (c) Sakanoue, K.; Motoda, M.; Sugimoto, M.; Sakaki, S. *J. Phys. Chem. A* **1999**, *103*, 5551–5556. (d) Lee, Y. Z.; Chen, X. W.; Chen, S. A.; Wei, P. K.; Fann, W. S. *J. Am. Chem. Soc.* **2001**, *123*, 2296–2307.

(32) Hutchison, G. R.; Ratner, M. A.; Marks, T. J. *J. Am. Chem. Soc.* **2005**, *127*, 2339–2350.

(33) (a) Li, X. N.; Liu, X. J.; Wu, Z. J.; Zhang, H. J. *J. Phys. Chem. A* **2008**, *112*, 11190–11197. (b) Li, X. N.; Feng, J. K.; Ren, A. M. *Chin. J. Chem.* **2008**, *26*, 1979–1984. (c) Liu, Y. L.; Feng, J. K.; Ren, A. M. *J. Phys. Org. Chem.* **2007**, *20*, 600–609.

(34) Yang, B.; Kim, S. K.; Xu, H.; Park, Y.; Zhang, H. Y.; Gu, C.; Shen, F. Z.; Wang, C. L.; Liu, D. D.; Liu, X. D.; Hanif, M.; Tang, S.; Li, W. J.; Li, F.; Shen, J. C.; Park, J. W.; Ma, Y. G. *ChemPhysChem* **2008**, *9*, 2601–2609.

(35) Yang, L.; Ren, A. M.; Feng, J. K.; Liu, X. J.; Ma, Y. G.; Zhang, M.; Liu, X. D.; Shen, J. C.; Zhang, H. X. *J. Phys. Chem. A* **2004**, *108*, 6797–6808.

(36) Burrows, P. E.; Shen, Z.; Bulovic, V.; McCarty, D. M.; Forrest, S. R.; Cronin, J. A.; Thompson, M. E. *J. Appl. Phys.* **1996**, *79*, 7991–8006.

Table 3. Calculated Absorption of **1**−**5** in CH_2Cl_2 Media at TD-B3LYP Level, Together with Experimental Values

	states	λ(nm) /E(eV)	oscillator	main configurations	assign	exptl[16]
1	S_1	391/3.17	0.0132	H→L(74%)	Ir/pta/ph→F_2-ppy (MLCT/LLCT)	
	S_4	375/3.30	0.0665	H→L+2(58%)	Ir/pta/ph→F_2-ppy/pta (MLCT/LLCT/ILCT)	370
	S_{15}	308/4.03	0.0896	H-2→L+1(50%)	Ir/F_2-ppy→F_2-ppy/pta (MLCT/LLCT/ILCT)	315
	S_{17}	303/4.09	0.1562	H-3→L+2(38%)	Ir/F_2-ppy→F_2-ppy/pta (MLCT/LLCT/ILCT)	
	S_{21}	294/4.22	0.1911	H-4→L+1(47%)	ph→F_2-ppy/pta (LLCT)	280
	S_{33}	267/4.64	0.4057	H→L+6(45%)	Ir/pta/ph→pta/ph (MLCT/ ILCT)	
	S_{34}	266/4.65	0.1685	H-2→L+4(51%)	Ir/F_2-ppy→F_2-ppy/pta (MLCT/LLCT/ILCT)	258
	S_{35}	266/4.67	0.1197	H-4→L+3(29%)	ph→F_2-ppy (LLCT)	
2	S_1	397/3.12	0.0066	H→L(91%)	pta/Me-ph→F_2-ppy (LLCT)	
	S_4	380/3.26	0.0726	H→L+2(76%)	pta/Me-ph→F_2-ppy/pta (LLCT/ILCT)	370
	S_{16}	305/4.07	0.1196	H-2→L+2(37%)	Ir/F_2-ppy→F_2-ppy/pta (MLCT/LLCT/ILCT)	315
	S_{21}	294/4.21	0.1941	H-4→L+1(44%)	Me-ph→F_2-ppy/pta (LLCT)	
	S_{33}	270/4.60	0.5015	H→L+6(38%)	pta/Me-ph→F_2-ppy/pta(LLCT/ILCT)	281
	S_{36}	266/4.65	0.2108	H-2→L+4(36%)	Ir/F_2-ppy→F_2-ppy/pta(MLCT/LLCT/ILCT)	259
	S_{37}	265/4.67	0.1895	H-2→L+4(21%)	Ir/F_2-ppy→F_2-ppy/pta (MLCT/LLCT/ILCT)	
3	S_1	388/3.20	0.0305	H→L(90%)	Ir/F_2-ppy/pta/F_2-ph→F_2-ppy (MLCT/LLCT/ILCT)	
	S_5	354/3.50	0.0901	H-1→L+1(95%)	Ir/F_2-ppy/pta→F_2-ppy/pta (MLCT/LLCT/ILCT)	370
	S_8	318/3.90	0.0671	H-2→L(68%)	Ir/F_2-ppy→F_2-ppy (MLCT/ILCT)	315
	S_{20}	294/4.22	0.1461	H-1→L+5(51%)	Ir/F_2-ppy/pta→F_2-ppy/pta (MLCT/LLCT/ILCT)	282
	S_{33}	268/4.63	0.1672	H→L+6(88%)	Ir/F_2-ppy/pta/F_2-ph→pta/F_2-ph (MLCT/LLCT/ILCT)	
	S_{35}	265/4.67	0.2339	H-2→L+4(53%)	Ir/F_2-ppy→F_2-ppy/pta (MLCT/LLCT/ILCT)	256
	S_{38}	262/4.72	0.1237	H-1→L+6(68%)	Ir/F_2-ppy/pta→pta/F_2-ph (MLCT/LLCT/ILCT)	
	S_{47}	254/4.88	0.1725	H→L+7(21%)	Ir/F_2-ppy/pta/F_2-ph→Ir/F_2-ppy (d-d/MLCT/LLCT/ILCT)	
4	S_1	384/3.23	0.0389	H→L (66%)	Ir/F_2-ppy→F_2-ppy/pta (MLCT/LLCT/ILCT)	
				H→L+1 (34%)	Ir/F_2-ppy→F_2-ppy/pta (MLCT/LLCT/ILCT)	
	S_{16}	298/4.17	0.1042	H-4→L(46%)	Ir/F_2-ppy/pta→F_2-ppy/pta (MLCT/LLCT/ILCT)	
	S_{27}	274/4.53	0.1528	H-2→L+3 (37%)	F_2-ppy/pta→F_2-ppy/pta (ILCT)	
	S_{31}	262/4.83	0.1032	H-4→L+3(42%)	Ir/F_2-ppy/pta→F_2-ppy/pta (MLCT/LLCT/ILCT)	
				H-2→L+4 (41%)	F_2-ppy/pta→F_2-ppy/pta (ILCT)	
	S_{32}	261/4.75	0.1088	H-2→L+4 (25%)	F_2-ppy/pta→F_2-ppy/pta (ILCT)	
				H-4→L+3 (23%)	Ir/F_2-ppy/pta→F_2-ppy/pta (MLCT/LLCT/ILCT)	
	S_{38}	252/4.91	0.1527	H-1→L+8 (20%)	Ir/F_2-ppy/pta→Ir/F_2-ppy (d-d/MLCT/LLCT/ILCT)	
5	S_1	383/3.24	0.0363	H→L (62%)	Ir/F_2-ppy→F_2-ppy/pyN4 (MLCT/LLCT/ILCT)	
				H→L+1 (38%)	Ir/F_2-ppy→F_2-ppy/pyN4 (MLCT/LLCT/ILCT)	
	S_8	316/3.93	0.0886	H-1→L+2(59%)	Ir/F_2-ppy/pyN4→F_2-ppy (MLCT/LLCT/ILCT)	
	S_{16}	296/4.18	0.1247	H-3→L+2(43%)	Ir/F_2-ppy→F_2-ppy (MLCT/ILCT)	
	S_{17}	294/4.22	0.1170	H-4→L+1(73%)	Ir/F_2-ppy/pyN4→F_2-ppy/pyN4 (MLCT/LLCT/ILCT)	
	S_{26}	271/4.58	0.1172	H-2→L+3(53%)	Ir/F_2-ppy/pyN4→F_2-ppy/pyN4 (MLCT/LLCT/ILCT)	
	S_{30}	265/4.69	0.1388	H-6→L+2(56%)	Ir/F_2-ppy/pyN4→F_2-ppy (MLCT/LLCT/ILCT)	
	S_{34}	258/4.80	0.1390	H→L+8(32%)	Ir/F_2-ppy→Ir/F_2-ppy (d-d/MLCT /ILCT)	
				H→L+6(29%)	Ir/F_2-ppy→F_2-ppy (MLCT/ILCT)	
	S_{38}	252/4.92	0.1800	H→L+6(19%)	Ir/F_2-ppy→F_2-ppy (MLCT/ILCT)	

on the ligand [π(pta+Me-ph)→π^*(F_2-ppy)]. Figure 5 indicates that the first distinguishable absorption bands show a similar energy variation trend to those of the lowest lying absorptions, while these absorptions for **4** and **5** are very weak. In Table 3, the calculated values of these bands are localized at 375, 380, and 354 nm for **1**−**3**, respectively, which correspond well to the experimental value of 370 nm. For **1** and **3**, the transition can be ascribed as mixed character of MLCT/LLCT/ILCT {[d_{xz}(Ir)+π(pta+ph)→π^*(F_2-ppy+pta)] for **1** and [d_{z^2}(Ir)+d_{xy}(Ir)+π(F_2-ppy+pta)→π^*(F_2-ppy+pta)] for **3**}. While the LLCT and ILCT [π(pta+Me-ph)→π^*(F_2-ppy+pta)] is the main character for the 380 nm absorption of **2**, perturbed by a small MLCT components as can be seen from Table S2, Supporting Information.

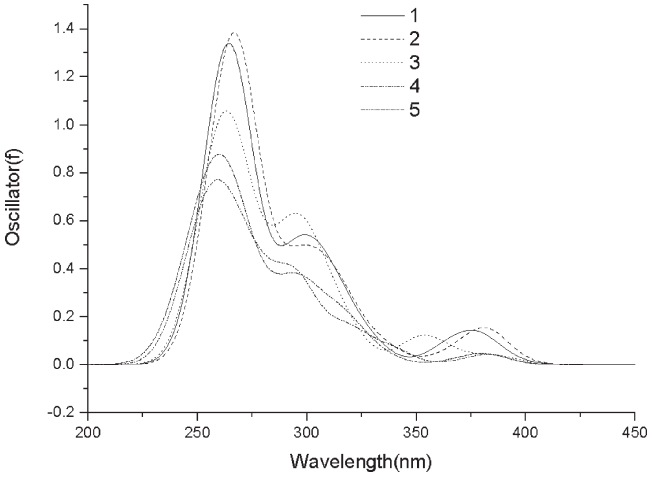

Figure 5. Simulated absorption spectra of **1**−**5** in CH_2Cl_2 media with the calculated data under the TD-B3LYP/LANL2DZ level.

In experiment, the higher absorption peaks close to the highest ones are not well separated.[16] It is thus the advantage of the theoretical study to separate these peaks. In Figure 5, the second distinguished absorption bands appear at 280−340 nm. For all the five complexes, the transitions with the largest oscillator strengths located at around 295 nm dominate these higher-energy absorption bands. The transition configuration of HOMO−4→LUMO+1 contributes to the 294 nm absorption of **1** and **2**, while the HOMO−1→LUMO+5 excitation is the main configuration for **3**. In combination with Table 3 and Tables S1−S5, Supporting Information, HOMO−4 of **1** and **2** is mainly π(ph/Me-ph) orbital, and LUMO+1

Table 4. Phosphorescent Emissions of **1**−**5** in CH_2Cl_2 Solution under the TDDFT Calculations, Together with the Experimental Values

complex	λ(nm)/E(eV)	major configuration	character	exptl[16,17]
1	532/2.33	L→H(90%)	pta→pta/ph(LLCT/ILCT)	489
2	538/2.31	L→H(88%)	pta→pta/Me-ph(LLCT/ILCT)	492
3	504/2.46	L→H(43%)	F_2-ppy→F_2-ppy/pta(LLCT/ILCT)	490
		L→H-2(49%)	F_2-ppy→F_2-ppy/pta(LLCT/ILCT)	
4	504/2.46	L→H(45%)	F_2-ppy→Ir/ F_2-ppy(MLCT/LLCT)	489
		L→H-1(36%)	F_2-ppy→ F_2-ppy(ILCT)	
5	506/2.45	L→H-1(49%)	F_2-ppy→ F_2-ppy(ILCT)	489
		L→H(48%)	F_2-ppy→ F_2-ppy(ILCT)	

is π^*(F_2-ppy+pta) orbital in nature. Therefore, the LLCT [π(ph/Me-ph)→π^*(F_2-ppy+pta)] is the main transition character for these excitations, while the MLCT/LLCT/ILCT is the main transition character for **3** and **4** [d(Ir)+π(F_2-ppy+pta) →π^*(F_2-ppy/pta)]. For **5**, the transition is mainly MLCT and ILCT in nature [d(Ir)+π(F_2-ppy) →π^*(F_2-ppy)], and the pyN4 moiety does not participate in this transition.

The observed strongest absorptions located at the highest energy regions are 258, 259, and 256 nm for **1**−**3**, respectively.[16] The calculated results in CH_2Cl_2 solution are 267, 270, 265, 252, and 258 nm for **1**−**5**, which agree well with the measured absorptions in terms of the absolute values and the trends, and they are again blue-shifted in the order **4** < **5** < **3** < **1** < **2**. The absorption at 267 nm for **1** is mainly contributed by the HOMO→LUMO+6 configuration, has the largest oscillator strength of 0.4057 (Figure 5), and is attributed to the [d_{xz}(Ir)+π(pta+ph/4F-ph) →π^*(pta+ph/4F-ph)] transition with the character of MLCT and ILCT. For the 270 and 265 nm absorptions, HOMO [π(pta+Me-ph)]→LUMO+6[π^*(F_2-ppy+pta)](LLCT/ILCT) and HOMO−2 [(d(Ir)+π(F_2-ppy)]→LUMO+4[π^*(F_2-ppy+pta)](MLCT/LLCT/ILCT) are the main configurations. For **4** and **5**, the calculated 252 (0.1527) and 258 nm (0.1390) absorptions are in large blue-shifted compared with those of **1**−**3**. Similar to the first and the second absorption bands, the general absorption intensity of **4** and **5** are lower than those of **1**−**3**. The reasons for this difference in absorption intensity between **4**−**5** and **1**−**3** can be ascribed to the presence of metal-centered d-d non-radiative transition in **4** and **5**, which is not found in **1**−**3**. In addition, we noted that the transition from ancillary ligand in the higher energy region has vanished in **5**, which is due to the weakened Ir-ancillary interaction. This is consistent with the observation in the geometry structure section that the Ir-ancillary bond lengths are longer relative to those of the Ir−F_2-ppy moiety. The other higher energy absorptions have LLCT and/or ILCT character and can be ascribed to the intraligand π→π^* transitions. The absorptions of the isolated ligands F_2-ppy, pta-ph, pta-Me-ph, pta-F_2-ph, CF_3-pta, and pyN4 were obtained, and the simulated absorption spectra are presented in Figure S1, Supporting Information. The calculated vertical triplet absorptions of these complexes are at 452, 458, 459, 433, and 434 nm (Table S6, Supporting Information), respectively, having the transition characters of MLCT, LLCT, and ILCT. In the experiment, there is a broad absorption band at 340−450 nm, and the combined ^{1}MLCT and ^{3}MLCT transitions are responsible for it. However, we can not exclude the participation of S_0→T_1 transitions in the higher-energy regions, even though it is assumed that their contribution should decrease with the decreased wavelength.

From the above calculations, we come to the conclusions: (a) $-CF_3$ attached directly to the pta or the enhanced interannular π-conjugation of tetrazolate ring can weaken the metal ligand bond strength in **4** and **5**, which is expected for d-d radiationless deactivation. By contrast, the phenyl ring on pta can enhance the π-conjugation of the pta moiety and strengthens the metal−ligand bond strength, and therefore enhances the transition strength; (b) generally, substituents on the ending phenyl ring have a slight effect on the excited energy because the distance between the substituents and the pta ligand is interrupted by the phenyl moiety; (c) the electron-donating group can cause a red shift and electron-withdrawing groups can cause a blue shift of the excited energy; (d) the participation of the MLCT components in the absorption is usual and weak in the lower energy, but it is a very efficient process to collect light energy. The presence of singlet→triplet transitions confirms that spin-selection rules are not strictly obeyed for third-row transition-metal complexes. Therefore, in the emission process, the singlet→triplet intersystem crossing can also be very easy and ensured that Ir-centered complexes exhibited more efficient, room-temperature phosphorescence in both fluid and solid states than other transition metal complexes.

Phosphorescence Spectra. On the basis of the triplet excited-state geometries, we obtained the emission spectra of **1**−**5** in CH_2Cl_2 solution, and the results are listed in Table 4, associated with the emissive energies, assignments, and the experimental values. The plots of the molecular orbitals related to emissions of **1**−**5** are presented in Figure 6. Partial compositions of FMOs related to emission are listed in Table S7, Supporting Information.

Table 4 shows that the calculated lowest energy emissions of the five complexes are localized at 532, 538, 504, 504, and 506 nm, respectively. The predicted emission wavelengths deviate from the experimental data by 43, 46, 14, 15, and 17 nm for **1**−**5**, respectively, which is comparable with the results reported recently.[13] The calculated Stokes shifts between the ^{3}MLCT absorption and lowest energy emission are 0.41, 0.39, 0.24, 0.40, and 0.41 eV for **1**−**5**, and they are larger compared with other investigations of 0.05, 0.06, 0.02, and −0.09 eV,[37] which indicates that the lowest lying emissions for **1**−**5** will be in a larger mixture of ligand-based ^{3}(π→π^*) transitions and metal-to-ligand charge transfer (^{3}MLCT).[8b] Our calculated

(37) Liu, T.; Xia, B. H.; Zhou, X.; Zhang, H. X.; Pan, Q. J.; Gao, J. S. *Organometallics* **2007**, *26*, 143–149.

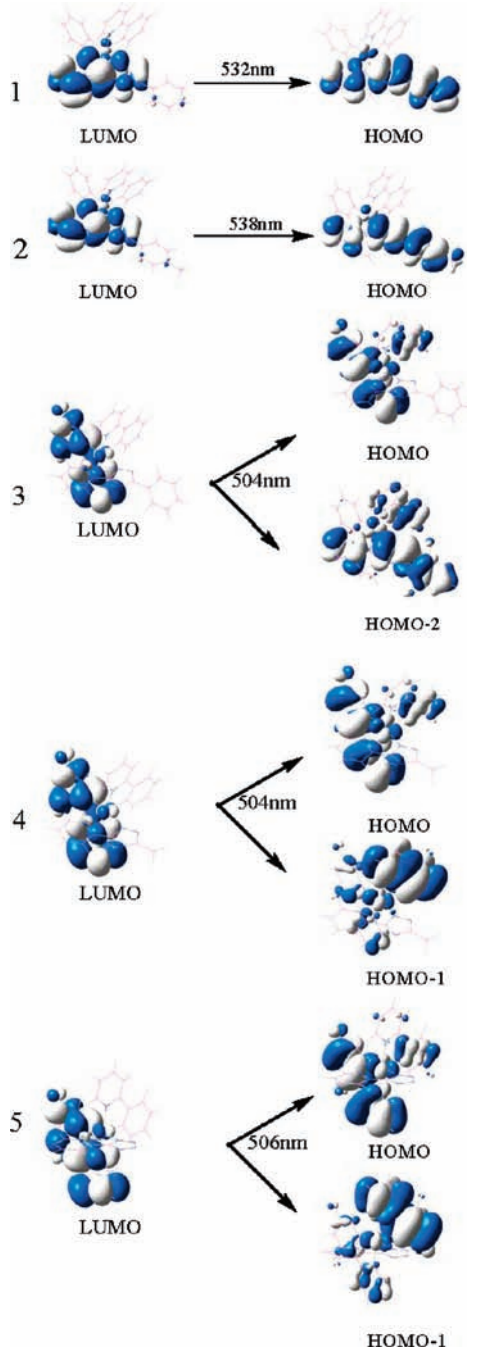

Figure 6. Singlet electron emission for **1**−**5**, calculated at TDDFT/B3LYP level in CH_2Cl_2 solution.

results agree well with the experimental observations that the measured emission spectra give highly structured emission[16,17] because emission bands from ^{3}MLCT states are generally broad and featureless, while $^3(\pi^*\rightarrow\pi)$ states typically give highly structured emissions.[8b] The efficient, high quantum yields of ligand-based phosphorescence are common in Ir complexes,[38] which makes the design of new phosphors straightforward by modification of the ligand structure.

Table 4 and Figure 6 show that the 532 and 538 nm emissions of **1** and **2** are mainly contributed by LUMO→HOMO transition configurations. In Table S7, Supporting Information, LUMO for **1** and **2** is mainly localized on the pta moiety, while the HOMO is localized exclusively on the ancillary ligand. Therefore, the transition characters of the 532 and 538 nm emissions can be described as ILCT/LLCT [π^*(pta)→π(pta+ph/Me-ph)]. For the 504 and 506 nm emissions of **3**−**5**, the configurations are nearly evenly contributed by the LUMO→HOMO$_{-n}$ (n = 0, 1, 2). Different from **1** and **2**, the LUMO of **3**−**5** resides primarily on the F_2-ppy moiety, while the HOMO$_{-n}$ is more delocalized with the composition from the F_2-ppy moiety, especially for **4** and **5**. Therefore, these emissions are attributed to ILCT and LLCT characters [π^*(F_2-ppy)→π(F_2-ppy)/ π(F_2-ppy+pta/F_2-ph)] for **3**, and ILCT character [π^*(F_2-ppy)→π(F_2-ppy)] for **4** and **5**. These different transition characters are consistent with the analysis of the geometry structure of the triplet excited states in the geometry structure section. The weakened interaction between the metal and the pta moiety decreases the F_2-ppy-based LUMO in **3**−**5** (Table S7, Supporting Information), and therefore, the HOMO benefits from the strengthened metal-F_2-ppy interaction.

Previous study has shown that the phosphorescence quantum efficiencies could be increased by a larger ^{3}MLCT composition, and the intersystem crossing could be enhanced by notable ^{3}MLCT participation. Namely, the $T_1\rightarrow S_0$ radiative transition should greatly increase the transition probability, hence shorten the radiative lifetime.[8b] A shorter phosphorescence lifetime while maintaining high quantum efficiencies requires a large radiative rate, which is directly proportional to the spin−orbit coupling (SOC) and singlet−triplet splitting (ΔE_{ST}).[39] Recently, it has been confirmed that MLCT character influences the ΔE_{ST} value, which in turn controls the radiative rate of the complexes.[40] For **3**−**5**, we found that the Ir d orbital composition is larger than **1** and **2**, and according to the above conclusion, **3**−**5** should have a higher radiative transition rate constant (k_r) among the five complexes; this is consistent with the measured higher k_r value of $2.7\times10^5 s^{-1}$ for **3** than that of 2.3 and $2.0\times10^5\ s^{-1}$ for **1** and **2**.[16] However, the quantum efficiency of **3** is only 0.16, which is lower than the 0.37 and 0.41 for **1** and **2**. This may be due to the increased non-radiative rate constant (k_{nr}) value, which in turn leads to a reduction of the overall quantum yield. Because quantum yield (Φ) can be affected by the competition between k_r and k_{nr}, namely, $\Phi = k_r/(k_r + k_{nr})$.[41] The measured k_{nr} value for **3** is $13.7\times10^5\ s^{-1}$, and they are 3.9 and $2.8\times10^5 s^{-1}$ for **1** and **2**.[16] This greatly increased k_{nr} value for **3** can be ascribed to the weakened Ir−Npta bond and the distortion between pta and ending phenyl ring, which facilitates the non-radiative decay

(38) Dedeian, K.; Shi, J.; Shepherd, N.; Forsythe, E.; Morton, D. C. *Inorg. Chem.* **2005**, *44*, 4445–4447.

(39) Yersin, H. *Top. Curr. Chem.* **2004**, *241*, 1–26.

(40) Haneder, S.; Da Como, E.; Feldmann, J. M.; Lupton, J.; Lennartz, C.; Erk, P.; Fuchs, E.; Molt, O.; Münster, I.; Schildknecht, C.; Wagenblast, G. *Adv. Mater.* **2008**, *20*, 3325–3330.

(41) (a) De Angelis, F.; Fantacci, S.; Evans, N.; Klein, C.; Zakeeruddin, S. M.; Moser, J. E.; Kalyanasundaram, K.; Bolink, H. J.; Grätzel, M.; Nazeeruddin, M. K. *Inorg. Chem.* **2007**, *46*, 5989–6001. (b) Fantacci, S.; De Angelis, F.; Sgamellotti, A.; Marrone, A.; Re, N. *J. Am. Chem. Soc.* **2005**, *127*, 14144–14145. (c) Lo, S. C.; Shipley, C. P.; Bera, R. N.; Harding, R. E.; Cowley, A. R.; Burn, P. L.; Samuel, I. D. W. *Chem. Mater.* **2006**, *18*, 5119–5129. (d) Yang, C. H.; Li, S. W.; Chi, Y.; Cheng, Y. M.; Yeh, Y. S.; Chou, P. T.; Lee, G. H.; Wang, C. H.; Shu, C. F. *Inorg. Chem.* **2005**, *44*, 7770–7780.

channels and makes the metal-centered (MC) decay goes downward. The e_g*-like orbital occurs at LUMO+8, LUMO+10, LUMO+7, LUMO+8, and LUMO+8 for **1**−**5**, respectively. Such low MC states in **3** will enhance the radiationless deactivation and quench the emission in the triplet states, and we believe that this is the main reason for the resulting lower quantum yields of **3**. The absence of this torsion can significantly enhance the quantum yield of 0.29 and 0.41 for 4g and 4h as listed in literature.[16] The quantum yield of **4** can not be determined in experiment,[42] and the lower quantum efficiency for **4** and **5** results from the similar reason to **3**.

Conclusions

This theoretical work reported the investigation of geometrical structures, absorptions, injection, and transport abilities, phosphorescence mechanism of five blue-emitting iridium(III) cyclometalated complexes. The calculated results reveal that the phenyl-ring substituted complexes **1**−**3** have generally the higher HOMO and LUMO energies than those of **4** and **5**, which will consequently results in the easier hole injections into **1** and **3**, and the easier electron injections into **4** and **5**. The ionization potentials (IPs) and electron affinities (EAs) calculation demonstrated this fact. The internal reorganization energy calculation reveals that the hole transport abilities of these complexes are generally worse than for electron transport, while the difference between hole and electron transport is rather small compared with other photoluminescent transition-metal or organic molecules; therefore, they can act as emitters in OLEDs. The transition characters of the phosphorescence are mainly ligand-centered $\pi \rightarrow \pi^*$ transitions, which make the design of phosphors straightforward by modification of the ligand structure. The lower quantum yields of **3**−**5** than **1** and **2** in the experiments result from the weakened metal−ligand interaction, which can make the metal-center (MC) decay go downward.

Acknowledgment. The authors are grateful to the financial aid from the National Natural Science Foundation of China (Grants 20490210, 20631040, 20602035, and 20771099) and the MOST of China (Grants 2006CB601103 and 2006DFA42610). (Grants 20631040 and 20771099) and the MOST of China (Grants 2006CB601103).

Supporting Information Available: The frontier molecular orbital compositions in the ground state for **1**−**5** at the DFT/B3LYP level are listed in Tables S1−S5, the $S_0 \rightarrow T_1$ absorptions of the five complexes is listed in Table S6, the partial molecular orbital compositions (%) of the complexes in the excited states are listed in Table S7, the simulated absorption spectra for main ligand F_2-ppy and ancillary ligands pta-ph, pta-Me-ph, pta-F_2-ph, pta-CF_3 and pyN4 is presented in Figure S1. This material is available free of charge via the Internet at http://pubs.acs.org.

(42) Mak, C. S. K.; Hayer, A.; Pascu, S. I.; Watkins, S. E.; Holmes, A. B.; Köhler, A.; Friend, R. H. *Chem. Commun.* **2005**, 4708–4710.